An NMR-based docking model for the physiological transient complex between cytochrome *f* and cytochrome c_6

Irene Díaz-Moreno[a,b], Antonio Díaz-Quintana[a], Marcellus Ubbink[b], Miguel A. De la Rosa[a,*]

[a] *Instituto de Bioquímica Vegetal y Fotosíntesis, Universidad de Sevilla y Consejo Superior de Investigaciones Científicas, Américo Vespucio 49, 41092 Sevilla, Spain*
[b] *Leiden Institute of Chemistry, Leiden University, Gorlaeus Laboratories, P.O. Box 9502, 2300 RA Leiden, The Netherlands*

Received 22 February 2005; revised 11 April 2005; accepted 11 April 2005

Available online 27 April 2005

Edited by Peter Brzezinski

Abstract The physiological transient complex between cytochrome *f* (C*f*) and cytochrome c_6 (Cc_6) from the cyanobacterium *Nostoc* sp. PCC 7119 has been analysed by NMR spectroscopy. The binding constant at low ionic strength is $8 \pm 2\ mM^{-1}$, and the binding site of Cc_6 for C*f* is localized around its exposed haem edge. On the basis of the experimental data, the resulting docking simulations suggest that Cc_6 binds to C*f* in a fashion that is analogous to that of plastocyanin but differs between prokaryotes and eukaryotes.

Keywords: Cytochrome c_6; Cytochrome *f*; Transient interactions

1. Introduction

The electron transfer (ET) between the photosynthetic membrane complexes cytochrome b_6f and photosystem I (PSI) is performed via transient interactions by either cytochrome c_6 (Cc_6) or plastocyanin (Pc). The two soluble redox proteins have different structures, but they share common properties that seem to have undergone parallel variations throughout evolution [1,2]. Thus, the interactions between those proteins and their membrane partners represent an excellent system for comparative studies of transient complex formation. The ET from Pc and Cc_6 to PSI has been extensively studied in a wide variety of organisms, and kinetic data were used to establish a classification of the various reaction mechanisms [1,2]. Kinetic analyses, site-directed mutagenesis [2,3] and structural studies by NMR spectroscopy [4] have led to the identification of the residues of Cc_6 involved in its interaction with PSI. Also, the ET between the soluble domain of cytochrome *f* (C*f*) and Pc has been studied extensively [1], highlighting the role of electrostatic and hydrophobic interactions in binding [1]. NMR studies have enabled the determination of the relative orientations of Pc and C*f* in several Pc–C*f* complexes [5–10]. These studies demonstrate that the position of Pc within the complex is dependent on the extent of electrostatic interactions.

Experimental data concerning the interaction of Cc_6 and C*f* are scarce [1]. A fast-kinetics study using a Zn-Cc_6 derivative has been recently reported [11]. The only structural data correspond to cross-complexes between proteins from different sources [12,13]. Here, we report a study of the interaction between both cytochromes, isolated from the same organism, by chemical-shift perturbation mapping and docking approaches based on ambiguous interface restraints [14]. To our knowledge, this is the first structural analysis of a physiological Cc_6–C*f* complex by NMR spectroscopy.

2. Materials and methods

2.1. Protein preparation

Uniformly ^{15}N-labelled *Nostoc* sp. PCC 7119 Cc_6 was purified as described [10] from *Escherichia coli* cells transformed with both pEAC-WT [15] and pEC86 [16] plasmids. Production and purification of the soluble domain of *Nostoc* sp. PCC 7119 C*f* will be described elsewhere (Albarrán et al., submitted).

2.2. NMR samples

All samples contained 10 mM sodium phosphate, pH 6.0, and 5% D_2O. C*f* was reduced by ascorbate. The binding affinity between Cc_6 and C*f* was estimated by titration of 0.2 mM ^{15}N-labelled Cc_6 with a 3.7 mM C*f* solution. The effect of ionic strength was investigated by adding concentrated NaCl to a C*f*–Cc_6 sample with a [C*f*]/[Cc_6] ratio of 3.

2.3. NMR spectroscopy

2D ^{1}H–^{15}N heteronuclear single-quantum coherence (HSQC) spectra were recorded at 298 K on a Bruker DMX 600 NMR spectrometer. The spectral widths were 26.5 ppm (^{15}N) and 11.5 ppm (^{1}H). Data were processed with AZARA (www.bio.cam.ac.uk/azara), and the resulting spectra were analysed with Ansig for Windows [17]. The spectra were calibrated against the internal standard ^{15}N-acetamide (0.5 mM). Amide assignments of the *Nostoc* Cc_6 were taken from Crowley et al. [12].

2.4. Binding curves

All titration curves were fitted simultaneously to a 1:1 binding model [18] in order to get a single K_A value. Non-linear least-squares fits were performed in Origin 6.0 (Microcal Inc., USA) using the chemical-shift perturbation and the C*f*/Cc_6 ratio as dependent and independent variables, respectively, and the binding constant (K_A) and the maximum chemical-shift change ($\Delta\delta_{max}$) as fitted parameters.

*Corresponding author. Fax: +34 954 460065.
E-mail address: marosa@us.es (M.A. De la Rosa).

Abbreviations: AIRs, ambiguous interaction restraints; Cc_6, cytochrome c_6; C*f*, cytochrome *f*; ET, electron transfer; HADDOCK, high ambiguity driven docking approach; HSQC, heteronuclear single-quantum coherence; Pc, plastocyanin; PSI, photosystem I; RMSD, root mean square deviation

0014-5793/$30.00
doi:10.1016/j.febslet.2005.04.031

Table 1
Active and passive residues, along with flexible segments, used in the definition of the AIRs for docking of Cc_6 and C*f*

Cc_6	
Active residues	S16, A19, L24, A57, K62, G63, R64, K66, E68
Passive residues	K22, K55, N56, P59, P67, E71
Flexible segments	9–9, 16–17, 24–25, 57–65
C*f*	
Active residues	–
Passive residues	Q7, P10, E11, R14, P16, T17, R19, L27, A29, P31, D55, S57, Q59, A63, D64, S66, K67, V68, Y102, Q104, E108, D109, P120, E122, Q123, T163, G164, E165, K166, D190
Flexible segments	1–7, 63–64, 96–97, 102–108, 114–118, 160–163, 188–191

2.5. Chemical-shift mapping

The shifts observed at the last titration point were extrapolated to 100% bound for all residues. The average chemical-shift perturbation ($\Delta\delta_{avg}$) of each amide was defined [19] as $[(\Delta\delta_N/5)^2 + (\Delta\delta_H)^2]^{1/2}$, where $\Delta\delta_N$ and $\Delta\delta_H$ are, respectively, the changes in the ^{15}N and ^{1}H chemical shifts when Cc_6 is 100% bound to C*f*.

2.6. Ambiguous interaction restraints

Ambiguous interaction restraints (AIRs) for the high ambiguity driven docking approach (HADDOCK) docking simulation were generated using standard criteria [14]. Residues labelled as 'active' (Table 1) were those showing $\Delta\delta_{Bind}$ of $^{1}H \geqslant 0.030$ or $^{15}N \geqslant 0.100$ ppm and a solvent accessibility, calculated with NACCESS [20], larger than 50%. For Cc_6, residues at less than 4 Å from the 'active' ones and showing high solvent accessible surface (>50%) were tagged as 'passive'. For C*f*, no 'active' residues were defined and 'passive' residues corresponded to those closer than 15 Å from the haem group and with a high solvent accessibility (>50%).

2.7. Docking protocol

Docking calculations were performed with the HADDOCK suite [14], using homology models of both proteins [3,10] as input. For each run, 2000 rigid-body solutions were generated by energy minimization, using an 8.5 Å non-bonded evaluation cut-off. The 100 structures with lowest AIR restraint energies were subjected to semi-flexible simulated annealing in torsion angle space [14] followed by a final refinement in explicit water [21]. Flexible segments were defined by the 'active' and 'passive' residues used in the AIRs ± 2 sequential amino-acids (Table 1). The non-bonded energies were calculated using the OPLS parameters [22].

2.8. Analysis

The 100 best structures were clustered according to pair-wise root mean square deviation (RMSD) of Cc_6 backbone atoms after aligning backbone atoms of C*f*. RMSD cut-off for clustering was 1.75 Å. Clusters were ranked according to their average interaction energies. The buried surface area was calculated as in [14], using a 1.4 Åprobe radius.

3. Results

To study the interactions between C*f* and Cc_6, a series of ^{15}N–^{1}H HSQC experiments was acquired on a solution of ^{15}N-labelled Cc_6 to which increasing amounts of C*f* were added. A number of Cc_6 amide signals shifted progressively during the titration with C*f* (Fig. 1). Hence, binding and dissociation are fast on the NMR timescale (>100 s^{-1}). A global fit of the data to a 1:1 binding model [18] yields a binding constant of 8 (±2) × 10^3 M^{-1}.

Fig. 2 shows a map of the Cc_6 residues affected by the titration of C*f*. Three stretches of primary structure surrounding the haem cleft are involved in binding to C*f*. Two of them (residues 9–20, except S11, and 23–27) form a hydrophobic patch in which C17 and V25 show the largest chemical-shift changes. The first stretch contains the haem-binding motif CXXCH, including the haem axial ligand H18. The third stretch showing significant $\Delta\delta_{Avg}$ (residues 52–65, except K55 and K62) includes the sixth iron ligand, M58. This residue, along with A60, experiences the largest perturbations of the stretch. No data are available for P59 (marked in grey in Fig. 2). It is noteworthy that E68, at the protein rear, exhibits a medium sized perturbation, like in the cross-complex between *Nostoc* Cc_6 and *Phormidium* C*f* [12].

To study the role of electrostatics in the Cc_6–C*f* complex, the salt effect on chemical-shift perturbations was investigated.

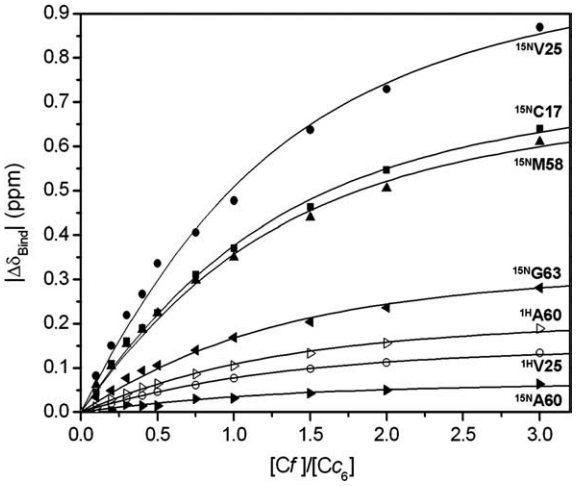

Fig. 1. Binding curves for the physiological interaction between *Nostoc* Cc_6 and C*f*. The absolute value of the chemical-shift perturbation of several amide signals is plotted as a function of the molar ratio of C*f* and Cc_6. Curves represent the best global fit to a 1:1 binding model with K_A = 8 (±2) × 10^3 M^{-1}.

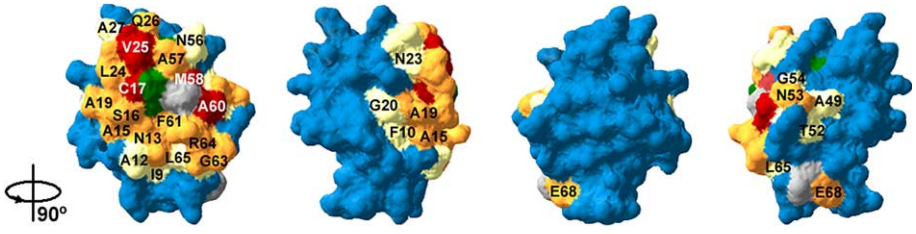

Fig. 2. Chemical-shift perturbation map of Cc_6 in the presence of C*f*. Residues are coloured according to their respective $\Delta\delta_{Avg}$ value (ppm), as follows: blue for <0.025, yellow for ⩽0.050, orange for ⩽0.125, and red for ⩽0.250. Prolines are in dark grey, and the haem group is in green.

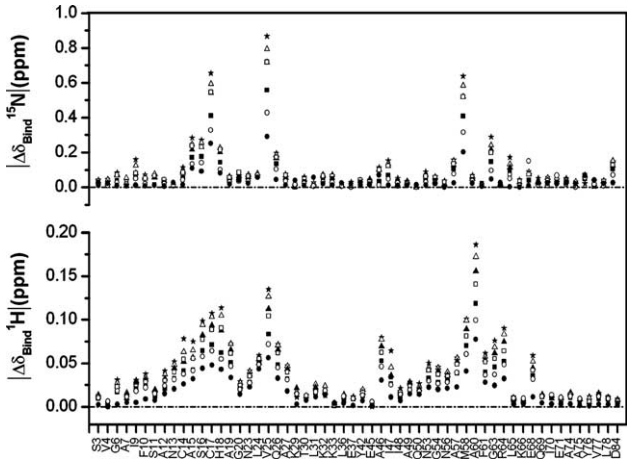

Fig. 3. Ionic strength dependence of $|\Delta\delta_{Bind}|$ for fifty-six affected backbone amide resonances, observed in the complex between Cc_6 and C*f*. The NaCl concentrations were: 0 mM (☆), 5 mM (△), 10 mM (▲), 20 mM (□), 40 mM (■), 80 mM (○), and 160 mM (●).

Fig. 3 shows that $\Delta\delta_{Bind}$ of all perturbed signals depends equally on ionic strength. Hence, the binding equilibrium is affected, but not the relative orientation of both partners in the complex. The residues showing the largest perturbation at low ionic strength still undergo appreciable shifts at 160 mM NaCl.

The NMR perturbation data were used to build a model of the complex using HADDOCK [14]. The 100 refined Cc_6–C*f* complex models, generated by these calculations, were organized in two clusters (Table 2), with their average RMSD to the lowest energy structure being 0.68 ± 0.13 and 1.09 ± 0.08 Å, respectively. Hence, the conformations of both clusters are not very different. In Table 2, E_{inter} (sum of intermolecular van der Waals, electrostatic and AIR energy terms) for the 100 refined complex structures is also shown. For both clusters, the energy term E_{AIR}, which is a measure for the disagreement between calculated structures and experimental restraints, is small, with values between 0.6 and 0.7 kcal mol^{-1}, indicative of a very low number of AIR violations per structure. The average values of buried surface area are in the range of that found in other complexes involving C*f* [5–10]. This is a standard size for non-obligate protein complexes [23–26]. The ensemble of the 10 best structures with the lowest intermolecular energy is shown in Fig. 4. Their average RMSD with respect to the lowest intermolecular energy structure is 0.71 ± 0.28 Å. The orientation of the proteins allows a distance between the two haem iron atoms of 18.0 ± 0.3 Å. The RMSD of backbone atoms is significantly higher for some residues at the interface, probably due to a local rearrangement of protein surface during docking [27].

Fig. 4. Structural model of the *Nostoc* Cc_6–C*f* complex. Tube representation is formed by the ten models with the lowest intermolecular energy after alignment of the C*f* molecules. The radius of the tube is proportional to the backbone RMSD of each residue.

In Fig. 5, the interface residues of the complex Cc_6–C*f* is represented. In Cc_6, the interface residues mainly belong to two stretches: 23–27 and, at the opposite side of the haem cleft, 52–65, which shows increased RMSD. Likewise, the C and N terminal domains show a high mobility. In C*f*, the residues at the interface also show increased RMSDs, and those in a turn at the small subunit (188–191) may have inherent flexibility.

It is known that charge interactions, at the interface edge, increase the binding constant in transient complexes [5,8]. In the model reported herein, residues K62 and K66 of Cc_6 are close to D64 and D190 of C*f*, respectively. Several others (K8 from Cc_6, and D190 from C*f*) are far away from each other, but could still contribute to long-range electrostatic interactions. R157 and a haem propionate of C*f* lie near R64 on Cc_6, as in the theoretical model [13]. The haem propionate may screen the repulsion between both basic residues.

Table 2
Statistical analysis of HADDOCK data after clustering the solutions for the *Nostoc* Cc_6–C*f* complex

	RMSD[a] (Å)	RMSD min[b] (Å)	Number of structures	E_{inter} (kcal mol^{-1})	E_{vdw} (kcal mol^{-1})	E_{elec} (kcal mol^{-1})	E_{AIR} (kcal mol^{-1})	Number of AIR violations ($\geqslant 0.1$ Å)	Buried surface area (Å^2)
Cluster 1	0.68 ± 0.13	0.68 ± 0.13	92	-253 ± 44	-53 ± 7	-201 ± 46	0.6 ± 1.0	0.3 ± 0.5	1683 ± 77
Cluster 2	0.63 ± 0.32	1.09 ± 0.08	5	-242 ± 24	-39 ± 3	-203 ± 26	0.7 ± 0.7	0.4 ± 0.5	1536 ± 26

Clusters are sorted according to average intermolecular energy.
$E_{inter} = E_{elec} + E_{vdw} + E_{AIR}$; where E_{elec}, E_{vdw} and E_{AIR} are the electrostatic, van der Waals and restraints energy terms, respectively.
[a]Average RMSD and standard deviation from the lowest energy structure of the cluster.
[b]Average RMSD and standard deviation from the lowest energy structure of all calculated structures.

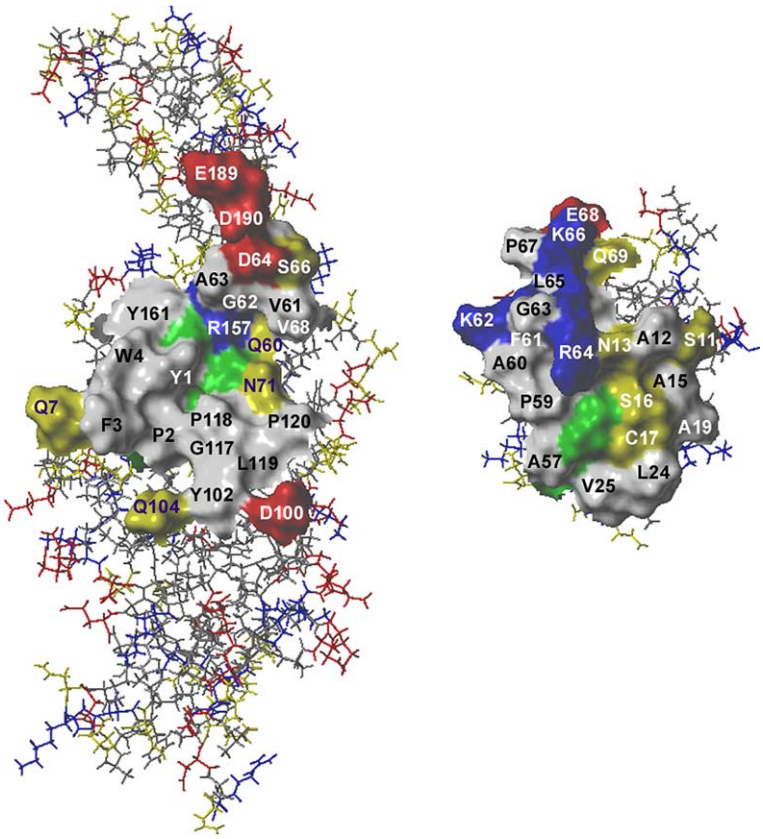

Fig. 5. Interface residues of the *Nostoc* Cc_6–C*f* complex. Cc_6 and C*f* are independently rotated 90° to the right and to the left, respectively, with regard to their orientation in the complex at Fig. 4. Residues are coloured according to their respective polarity, as follows: grey for hydrophobic, yellow for polar, blue and red for positively and negatively charged, respectively. Haem groups are in green.

Most of the interface corresponds to non-polar (61%) residues that account for 45% of the buried surface. The guanidyl of R64 and the haem propionates lay at the centre of the interface; this arginine accounts for 17% (150 Å^2) of Cc_6 buried surface and contributes to hydrophobic interactions through its side-chain. With the exception of R64, the interface core contains mainly hydrophobic residues, placed around both haem groups on Cc_6 and C*f*. Four prolines are located at the interface, namely P59 (56 Å^2 buried) and P67 (50 Å^2) from Cc_6 and P118 (40 Å^2) and P120 (21 Å^2) from C*f*. They account for 10% of buried surface. Several polar, uncharged residues (two asparagines and two glutamines) surround the small hydrophobic core and may enhance the dissociation rate by facilitating interface re-solvation [5,8,9]. With the exception of the buried charge of R64, the composition of the interface is typical of transient complexes [4,5,8,9,28,29].

4. Discussion

This work reports the first experimental data on the structure of a physiological Cc_6–C*f* complex. The observed binding constant is identical to that for the cross-complex between *Nostoc* Cc_6 and *Phormidium* C*f* ($K_A = 8 (\pm 2) \times 10^3$ M^{-1}) [12]. The chemical-shift perturbation map indicates that *Nostoc* Cc_6 binds to *Nostoc* and *Phormidium* C*f* in a similar way.

However, some significant differences are found between the homologous and heterologous complexes, probably due to an electrostatic bias in the cross-interaction. K55 and, strikingly, K80 – both from Cc_6 – show perturbations in the cross-complex but not in the native one, while the opposite holds for R64. Other studies [2–4] have emphasized the importance of R64, both functionally and structurally, for the interaction of Cc_6 with its other redox partner, PSI; the finding that R64 is involved in binding C*f* is in line with these results.

The position of Cc_6 with respect to C*f* in the models resulting from our calculations is similar to that from one of the two top ranking configurations of the *Nostoc* Cc_6–*Phormidium* C*f* complex [12] predicted by NMR filtered docking using BiGGER [30]. Both results resemble the models of the Cc_6–C*f* complex from the green alga *Chlamydomonas* [13] and of the cross-complex between turnip C*f* and *Monoraphidium* Cc_6 (PDB entry, 1JX8). In all these complexes, Cc_6 interacts with charged amino-acids at the small domain of C*f* (Fig. 6A). Positive charges on C*f* interact with negative charges on Cc_6 in green algae, but the opposite stands for cyanobacteria. A highly interesting finding is that Cc_6 is more distant from the small domain of C*f* in the *Nostoc* complex than in the *Monoraphidium*-turnip model, a difference that is similar to that between the conformations of the plant [8,9] and *Nostoc* [10] Pc–C*f* complexes (Fig. 6B). It, thus, seems that the relative orientation of both partners within the transient complex varies significantly from eukaryotes to

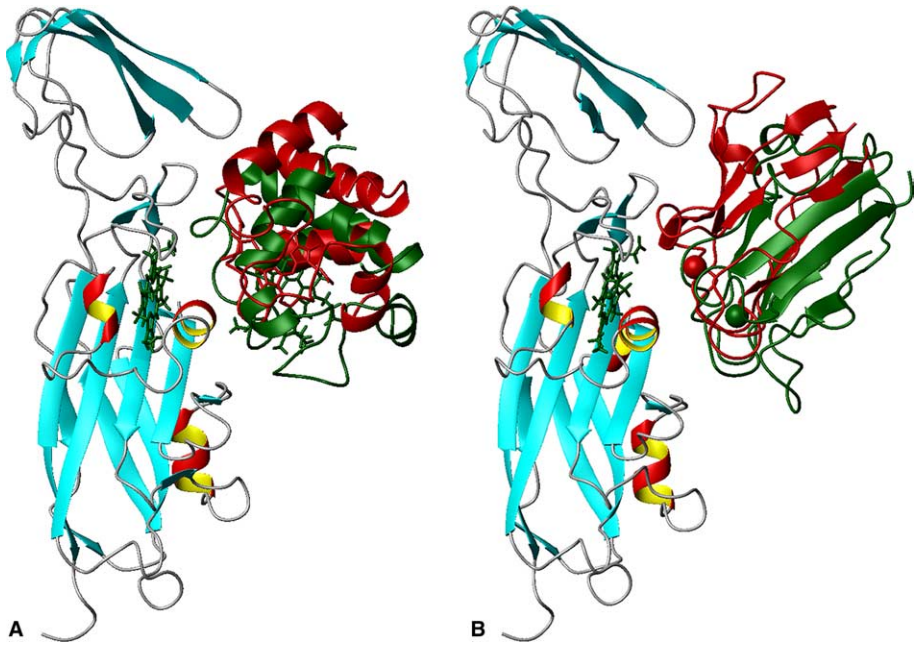

Fig. 6. Comparison between the C*f*–Cc_6 (A) and C*f*–Pc (B) complexes. With the lowest energy models of *Nostoc* complexes as references, C*f* is coloured according to its secondary structure whereas Cc_6 (in A) and Pc (in B) are coloured in green. *Monoraphidium* Cc_6 (in A) and spinach Pc (in B) in cross-complexes with turnip C*f* are both in red, for which turnip C*f* (not shown) is aligned with *Nostoc* C*f*. The structures in A are from this work, and from PDB (1JX8); those in B are also from PDB (2PCF and 1TU2).

prokaryotic organisms, in agreement with the previously observed kinetic differences.

Acknowledgements: This work was supported by the Programme Human Potential and Mobility of Researchers of the European Commission (Contract No. HPRN-CT-1999-00095), the Spanish Ministry of Education, Culture and Sport (Grant No. AP2000-2937), the Spanish Ministry of Science and Technology (Grant No. BMC2003-00458), the Andalusian Government (Grant PAI, CVI-0198) and the Netherlands Organisation for Scientific Research (Grant No. 700.52.425).

References

[1] Hope, A.B. (2000) Electron transfers amongst cytochrome *f*, plastocyanin and photosystem I: kinetics and mechanisms. Biochim. Biophys. Acta 1456, 5–26.
[2] Díaz-Quintana, A., Navarro, J.A., Hervás, M., Molina-Heredia, F.P., De la Cerda, B. and De la Rosa, M.A. (2003) A comparative structural and functional analysis of cyanobacterial plastocyanin and cytochrome c_6 as alternative electron donors to photosystem I. Photosynth. Res. 75, 97–110.
[3] Molina-Heredia, F.P., Díaz-Quintana, A., Hervás, M., Navarro, J.A. and De la Rosa, M.A. (1999) Site-directed mutagenesis of cytochrome c_6 from *Anabaena* sp. PCC 7119. Identification of surface residues of the hemeprotein involved in photosystem I reduction. J. Biol. Chem. 274, 33565–33570.
[4] Díaz-Moreno, I., Díaz-Quintana, A., Molina-Heredia, F.P., Nieto, P.M., Hansson, Ö., De la Rosa, M.A. and Karlsson, B.G. (2005) NMR analysis of the transient complex between membrane photosystem I and soluble cytochrome c_6. J. Biol. Chem. 280, 7925–7931.
[5] Crowley, P.B. and Ubbink, M. (2003) Close encounters of the transient kind: Protein interactions in the photosynthetic redox chain investigated by NMR spectroscopy. Acc. Chem. Res. 36, 723–730.
[6] Ubbink, M., Ejdebäck, M., Karlsson, B.G. and Bendall, D.S. (1998) The structure of the complex of plastocyanin and cytochrome *f*, determined by paramagnetic NMR and restrained rigid-body molecular dynamics. Structure 6, 323–335.
[7] Lange, C., Cornvik, T., Díaz-Moreno, I. and Ubbink, M. (2005). The transient complex of poplar plastocyanin with cytochrome *f*: effects of ionic strength and pH. Biochim. Biophys. Acta Bioenerg., in press.
[8] Prudêncio, M. and Ubbink, M. (2004) Transient complexes of redox proteins: structural and dynamic details from NMR studies. J. Mol. Recog. 17, 524–539.
[9] Ubbink, M. (2004) Complexes of photosynthetic redox proteins studied by NMR. Photosynth. Res. 81, 277–287.
[10] Díaz-Moreno, I., Díaz-Quintana, A., De la Rosa, M.A. and Ubbink, M. (2005). Structure of the complex between plastocyanin and cytochrome *f* from the cyanobacterium *Nostoc* sp. PCC 7119 as determined by paramagnetic NMR. J. Biol. Chem., in press.
[11] Grove, T.Ž. and Kostić, N. (2003) Metalloprotein association self-association, and dynamics governed by hydrophobic interactions: Simultaneous occurrence of gated and true electron-transfer reactions between cytochrome *f* and cytochrome c_6 from *Chlamydomonas reinhardtii*. J. Am. Chem. Soc. 125, 10598–10607.
[12] Crowley, P.B., Díaz-Quintana, A., Molina-Heredia, F.P., Nieto, P., Sutter, M., Haehnel, W., De la Rosa, M.A. and Ubbink, M. (2002) The interactions of cyanobacterial cytochrome c_6 and cytochrome *f*, characterized by NMR. J. Biol. Chem. 277, 48685–48689.
[13] Gross, E.L. and Pearson, D.C. (2003) Brownian dynamics simulations of the interaction of *Chlamydomonas* cytochrome *f* with plastocyanin and cytochrome c_6. Biophys. J. 85, 2055–2068.
[14] Dominguez, C., Boelens, R. and Bonvin, A.M.J.J. (2003) HADDOCK: a protein–protein docking approach based on biochemical or biophysical information. J. Am. Chem. Soc. 125, 1731–1737.
[15] Molina-Heredia, F.P., Hervás, M., Navarro, J.A. and De la Rosa, M.A. (1998) Cloning and correct expression in *Escherichia coli* of the *pet*E and *pet*J genes respectively encoding plastocyanin and cytochrome c_6 from the cyanobacterium *Anabaena* sp. PCC 7119. Biochem. Biophys. Res. Commun. 243, 302–306.
[16] Arslan, E., Schulz, H., Zufferey, R., Künzaler, P. and Thöny-Meyer, L. (1998) Overproduction of the *Bradyrhizobium japonicum c* -type cytochrome subunits of the cbb(3) oxidase in *Escherichia coli*. Biochem. Biophys. Res. Commun. 251, 744–747.
[17] Helgstrand, M., Kraulis, P., Allard, P. and Hard, T. (2000) Ansig for Windows: an interactive computer program for semiautomatic

assignment of protein NMR spectra. J. Biomol. NMR 18, 329–336.
[18] Kannt, A., Young, S. and Bendall, D.S. (1996) The role of acidic residues of plastocyanin in its interaction with cytochrome *f*. Biochim. Biophys. Acta 1277, 115–126.
[19] Grzesiek, S., Bax, A., Clore, G.M., Gronenborn, A.M., Hu, J.S., Kaufman, J., Palmer, I., Stahl, S.J. and Wingfield, P.T. (1996) The solution structure of HIV-1 Nef reveals an unexpected fold and permits delineation of the binding surface for the SH3 domain of Hck tyrosine protein kinase. Nat. Struct. Biol. 3, 340–345.
[20] Hubbard, S.J., Campbell, S.F. and Thornton, J.M. (1991) Molecular recognition. Conformational analysis of limited proteolytic sites and serine proteinase protein inhibitors. J. Mol. Biol. 220, 507–530.
[21] Linge, J.P., Williams, M.A., Spronk, C.A.E.M., Bonvin, A.M.J.J. and Nilges, M. (2003) Refinement of protein structures in explicit solvent. Proteins 50, 496–506.
[22] Jorgensen, W.L. and Tirado-Rives, J. (1998) The OPLS potential function for proteins. Energy minimization for crystals of cyclic peptides and Crambin. J. Am. Chem. Soc. 110, 1657–1666.
[23] Jones, S. and Thornton, J.M. (1996) Principles of protein–protein interactions. Proc. Natl. Acad. Sci. USA 93, 13–20.
[24] Jones, S. and Thornton, J.M. (1997) Analysis of protein–protein interaction sites using surface patches. J. Mol. Biol. 272, 121–132.
[25] Chakrabarti, P. and Janin, J. (2002) Dissecting protein recognition sites. Proteins 47, 334–343.
[26] Wodak, S.J. and Janin, J. (2003) Structural basis for macromolecular recognition. Adv. Prot. Chem. 61, 9–73.
[27] Arnesano, F., Banci, L., Bertini, I. and Bonvin, A.M.J.J. (2004) A docking approach to the study of copper trafficking proteins: interaction between metallochaperones and soluble domains of copper ATPases. Structure 12, 669–676.
[28] Díaz-Moreno, I., Díaz-Quintana, A., De la Rosa, M.A., Crowley, P.B. and Ubbink, M. (2005) Different modes of interaction in cyanobacterial complexes of plastocyanin and cytochrome *f*. Biochemistry 44, 3176–3183.
[29] Crowley, P.B. and Carrondo, M.A. (2004) The architecture of the binding site in redox protein complexes: implications for fast dissociation. Proteins 55, 603–612.
[30] Palma, P.N., Krippahl, L., Wampler, J.E. and Moura, J.J.G. (2000) BiGGER: a new (soft) docking algorithm for predicting protein interactions. Protiens 39, 372–384.